Disentanglement via entanglement: A unified method for Wannier localization

Anil Damle[*] and Lin Lin[†]

March 22, 2017

Abstract

The Wannier localization problem in quantum physics is mathematically analogous to finding a localized representation of a subspace corresponding to a nonlinear eigenvalue problem. While Wannier localization is well understood for insulating materials with isolated eigenvalues, less is known for metallic systems with entangled eigenvalues. Currently, the most widely used method for treating systems with entangled eigenvalues is to first obtain a reduced subspace (often referred to as disentanglement) and then to solve the Wannier localization problem by treating the reduced subspace as an isolated system. This is a multi-objective nonconvex optimization procedure and its solution can depend sensitively on the initial guess. We propose a new method to solve the Wannier localization problem, avoiding the explicit use of an an optimization procedure. Our method is robust, efficient, relies on few tunable parameters, and provides a unified framework for addressing problems with isolated and entangled eigenvalues.

Localized representations of electronic wavefunctions have a wide range of applications in quantum physics, chemistry, and materials science. They require significantly less memory to store, and are the foundation of so-called "linear scaling methods" [17, 10, 3] for solving quantum problems. They can also be used to analyze the chemical bonding in complex materials, interpolate the band structure of crystals, accelerate ground and excited state electronic structure calculations, and form reduced order models for strongly correlated many body systems [21].

In an effective single particle theory such as Kohn-Sham density functional theory (KS-DFT) [13, 18], the electronic wavefunctions are given by the (possibly generalized) eigenfunctions, denoted $\{\psi_i(\mathbf{r})\}$, of a self-adjoint Hamiltonian operator $\mathcal{H}$:

$$\mathcal{H}\psi_i(\mathbf{r}) = \varepsilon_i\psi_i(\mathbf{r}), \quad \varepsilon_i \in \mathcal{I}. \tag{1}$$

Here $\mathcal{I}$ is an interval that can be interpreted as an energy window that indicates the eigenfunctions of physical interest. These eigenfunctions are generally delocalized, *i.e.* have significant magnitude in large portions of the computational domain. The Wannier localization problem is as follows: find an approximately minimal set of orthonormal and localized

[*]Department of Mathematics, University of California, Berkeley, CA 94720, USA (damle@berkeley.edu)

[†]Department of Mathematics, University of California, Berkeley, CA 94720, USA and Computational Research Division, Lawrence Berkeley National Laboratory, Berkeley, CA 94720, USA (linlin@math.berkeley.edu)

functions $\{w_j\}$, which have significant magnitude on only a small portion of the computational domain, such that $\mathrm{span}\{\psi_j\}_{\varepsilon_i \in \mathcal{I}} \subseteq \mathcal{V}_w := \mathrm{span}\{w_j\}$. Following the convention in quantum physics, $\{w_j\}$ are called Wannier functions [30, 16, 2].

When the eigenvalues in $\mathcal{I}$ are *isolated*, *i.e.*

$$\inf_{\varepsilon_i \in \mathcal{I}, \varepsilon_{i'} \notin \mathcal{I}} |\varepsilon_i - \varepsilon_{i'}| > 0, \tag{2}$$

the Wannier localization problem has been studied extensively in mathematics and physics [16, 2, 25, 22, 15, 4, 12, 8, 26, 27, 6, 24, 5, 7]. Loosely speaking, for a class of Hamiltonions $\mathcal{H}$, one can construct exponentially localized Wannier functions such that $\mathcal{V}_w = \mathrm{span}\{\psi_i\}_{\varepsilon_i \in \mathcal{I}}$. The isolation condition is satisfied when treating valence bands of insulating systems.

When the isolation condition (2) is violated, the eigenvalues in $\mathcal{I}$ become *entangled*. Entangled eigenvalues appear ubiquitously in metallic systems, but also insulating systems when conduction bands or a selected range of valence bands are considered. The problem now becomes significantly more difficult: both identify a subspace $\mathcal{V}_w$ that admits a localized basis, and construct such a basis.

The most widely used method to construct localized functions in this scenario is a *disentanglement* procedure [29]. It first identifies $\mathcal{V}_w$ by minimizing a nonlinear "smoothness functional". Then it computes $\{w_i\}$ by minimizing a nonlinear "spread functional" [22]. In both problems the feasible set is nonconvex. While this two step method has been successfully applied to a number of applications [21], there is little mathematical understanding of the disentanglement procedure. Sensitive dependence on the initial guess along with a number of tunable parameters in the optimization formulation gives rise to a number of practical difficulties in using this method. Often, detailed knowledge of the underlying physical system is required to obtain physically meaningful results.

In this article, we propose a unified method to address the Wannier localization problem for both isolated and entangled cases. Instead of an initial "disentanglement" step, our method explicitly constructs a quasi-density matrix that "entangles" the eigenfunctions of interest with the rest of the eigenfunctions in a controlled manner. This has the effect of simultaneously identifying the subspace $\mathcal{V}_w$ and constructing the localized basis. For the isolated case our new method reduces to the prior selected columns of the density matrix (SCDM) method [6], and hence we still refer to our new, unified approach as SCDM.

The SCDM method has several significant advantages. First is its simplicity. There are no tunable parameters for the isolated case and only two parameters in the entangled case. Second, SCDM is constructed using standard linear algebra operations, which makes it easy to implement and parallelize. Third, SCDM is a deterministic, one-step procedure and does not require an initial guess. Hence, it will not get stuck at local minima as other nonconvex, nonlinear optimization methods may. Finally, SCDM unifies the treatment of molecules and crystals, while standard methods often require significantly more complex treatment for crystals. We provide an interface to the widely used `Wannier90` software package [23] and demonstrate the effectiveness of SCDM via several examples of real materials with isolated and entangled eigenvalues.

The SCDM method

We consider the effective one-body Schrödinger operator $\mathcal{H} = -\frac{1}{2}\Delta + V(\mathbf{r})$ in $\mathbb{R}^3$, and all eigenfunctions of interest $\psi_i(\mathbf{r}) \in L^2(\mathbb{R}^3)$. This corresponds to problems involving molecules

and nanoclusters, which require a simpler setup than our forthcoming discussion of crystals.

For the isolated case, without loss of generality we assume only the algebraically smallest N eigenvalues $\{\varepsilon_i\}_{i=1}^N$ are in the interval $\mathcal{I}$, and the corresponding eigenfunctions $\{\psi_i\}_{i=1}^N$ are orthonormal. Using the Dirac notation, the *density matrix* $P = \sum_{i=1}^N |\psi_i\rangle\langle\psi_i|$ is a rank N matrix that is the spectral projector associated with $\mathcal{H}$ onto the interval $\mathcal{I}$. Notably, its kernel $P(\mathbf{r},\mathbf{r}')$ decays rapidly as $|\mathbf{r}-\mathbf{r}'| \to \infty$ [17, 1]. Intuitively, if we can select a set of N points $\mathcal{C} = \{\mathbf{r}_i\}_{i=1}^N$ so that the corresponding column vectors of the kernel $\{P(\mathbf{r},\mathbf{r}_i)\}_{i=1}^N$ are the "most representative" and well conditioned column vectors of P, these vectors almost form the desired Wannier functions up to the orthonormality condition.

In order to select the set $\mathcal{C}$, we let $\Psi \in \mathbb{C}^{N_g \times N}$ denote the unitary matrix corresponding to a discrete representation of $\{\psi_{i,\mathbf{k}}(\mathbf{r})\}_{i=1}^N$ using their nodal values on N_g grid points. The corresponding discretized density matrix, still denoted by P, is given by $P = \Psi\Psi^*$. Conceptually, the most representative column vectors can be identified via a QR factorization with column-pivoting (QRCP) [11] applied to P. However, this is often impractical since P is prohibitively expensive even to construct and store in memory. The SCDM method [6] proposes that the set $\mathcal{C}$ can be equivalently computed via the QRCP of the matrix Ψ^* as

$$\Psi^*\Pi = QR \equiv Q\begin{bmatrix} R_1 & R_2 \end{bmatrix}. \tag{3}$$

Here Π is a permutation matrix, Q is a unitary matrix, $R_1 \in \mathbb{C}^{N \times N}$ is an upper triangular matrix, and $R_2 \in \mathbb{C}^{N \times (N_g - N)}$. The points $\mathcal{C} = \{\mathbf{r}_i\}_{i=1}^N$ can be directly identified from the first N columns of the permutation matrix Π.

Having chosen $\mathcal{C}$, we must now orthonormalize the localized column vectors $\{P(\mathbf{r},\mathbf{r}_i)\}_{i=1}^N$ without destroying their locality. Note that $P(\mathbf{r},\mathbf{r}_i) = \sum_{i'=1}^N \psi_{i'}(\mathbf{r})\Xi_{i',i}$ where $\Xi \in \mathbb{C}^{N \times N}$ has matrix elements $\Xi_{i,i'} = \psi_i^*(\mathbf{r}_{i'})$. One way to enforce the orthogonality is

$$w_i(\mathbf{r}) = \sum_{i'=1}^N \psi_{i'}(\mathbf{r})U_{i',i}, \quad U = \Xi(\Xi^*\Xi)^{-\frac{1}{2}}. \tag{4}$$

Here $U \in \mathbb{C}^{N \times N}$ is a unitary matrix and is referred to as a *gauge* in physics literature. The matrix square root transformation in Eq. (4) is called the Löwdin transformation [20] and may be equivalently computed using the orthogonal factors from the reduced SVD of Ξ.

Considering

$$(\Xi^*\Xi)_{i,i'} = \sum_{i''=1}^N \psi_{i''}(\mathbf{r}_i)\psi_{i''}^*(\mathbf{r}_{i'}) = P(\mathbf{r}_i,\mathbf{r}_{i'}), \tag{5}$$

the decay properties of P imply that $[P(\mathbf{r}_i,\mathbf{r}_{i'})]$ may be viewed as a localized $N \times N$ matrix. If the eigenvalues $(\Xi^*\Xi)^{-\frac{1}{2}}$ are bounded away from 0, then $(\Xi^*\Xi)^{-\frac{1}{2}}$ will itself be localized [1], and consequently $\{w_i\}_{i=1}^N$ will be localized, orthonormal Wannier functions.

For the entangled case, we extend the SCDM method by "entangling" the eigenfunctions of interest with additional eigenfunctions through the use of a quasi-density matrix

$$P = \sum_i |\psi_i\rangle f(\varepsilon_i)\langle\psi_i| = f(H), \tag{6}$$

where $f(\cdot)$ is a smooth function, $\mathcal{I}$ is a subset of the support set of f, and the summation is formally over *all* eigenfunctions of $\mathcal{H}$. From this perspective, the case of isolated band is associated with the choice $f(\varepsilon) = \mathbf{1}_{\mathcal{I}}(\varepsilon)$, the indicator function on the interval $\mathcal{I}$.

3

We now assume there is a number μ_c such that $\inf_i |\varepsilon_i - \mu_c|$ is very small or even zero. The following two scenarios of entangled eigenvalues appear most frequently in quantum physics, corresponding to the Wannier localization problem below and around a certain energy level (usually the Fermi energy) respectively [31]. In both cases $f(\epsilon)$ is large on the region of interest and smoothly decays to zero outside $\mathcal{I}$ in a manner controlled by a parameter σ (see Fig. 1).
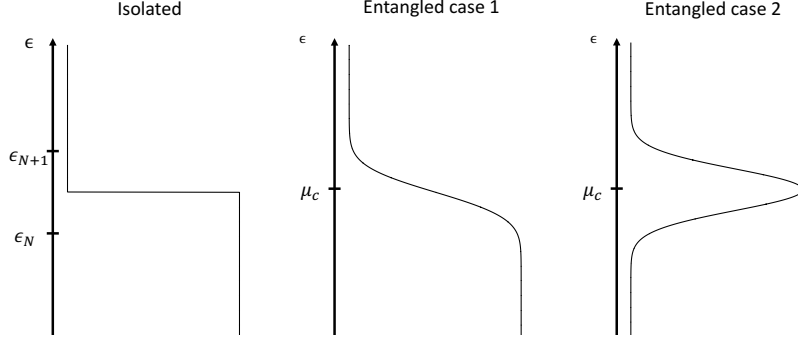
Figure 1: $f(\varepsilon)$ for the isolated and two entangled cases.

Entangled case 1: $\mathcal{I} = (-\infty, \mu_c)$. In this case we can choose a value $\sigma > 0$ and let

$$f(\varepsilon) = \frac{1}{2}\mathrm{erfc}\left(\frac{\varepsilon - \mu_c}{\sigma}\right) = \frac{1}{\sqrt{\pi\sigma^2}}\int_\varepsilon^\infty \exp\left(-\frac{(t - \mu_c)^2}{\sigma^2}\right)\,\mathrm{d}t. \tag{7}$$

The function $f(\varepsilon)$ satisfies $\lim_{\varepsilon \to -\infty} f(\varepsilon) = 1$, $\lim_{\varepsilon \to \infty} f(\varepsilon) = 0$ and the transition occurs smoothly around μ_c.

Entangled case 2: $\mathcal{I} = (\mu_c - \sigma, \mu_c + \sigma)$. In this case we choose f to be a Gaussian function

$$f(\varepsilon) = \exp\left(-\frac{(\varepsilon - \mu_c)^2}{\sigma^2}\right). \tag{8}$$

For a smooth function f, the kernel of the quasi-density matrix $P(\mathbf{r}, \mathbf{r}')$ also decays rapidly [1, 19], and we would once again like to select N_w "most representative" and well conditioned column vectors of P to construct the Wannier functions. Let $\mathcal{E} = \mathrm{diag}\left[\{\varepsilon_i\}\right] \in \mathbb{R}^{N \times N}$ be a diagonal matrix containing all eigenvalues such that $f(\varepsilon)$ is above some threshold, and $\Psi \in \mathbb{C}^{N_g \times N}$ be the matrix containing the corresponding discretized eigenvectors. We can now compute a QRCP for the weighted eigenvectors

$$(f(\mathcal{E})\Psi^*)\,\Pi = QR \tag{9}$$

and select the N_w columns corresponding to the left most N_w columns of the permutation Π. As before, we let $\mathcal{C} = \{\mathbf{r}_i\}_{i=1}^{N_w}$ denote the real space points corresponding to the selected columns and define the auxiliary matrix $\Xi \in \mathbb{C}^{N \times N_w}$ with $\Xi_{i,i'} = f(\varepsilon_i)\psi_i^*(\mathbf{r}_{i'})$. If the eigenvalues of $\Xi^*\Xi$ are bounded away from 0, the choice of gauge $U = \Xi(\Xi^*\Xi)^{-\frac{1}{2}}$ once again gives rise to the Wannier functions. Now, $U \in \mathbb{C}^{N \times N_w}$ is a rectangular matrix with orthonormal columns. Fig. 2 compares the delocalized eigenfunctions and the localized Wannier functions corresponding to isolated and entangled cases using a simple one-dimensional model problem, details of which are available in the supporting information.
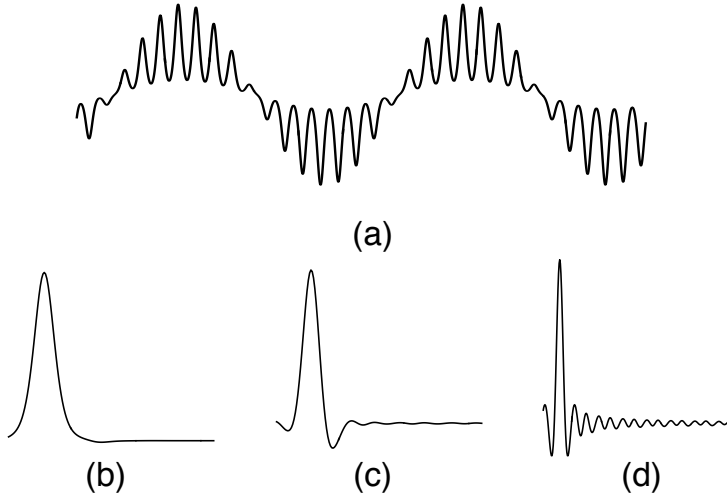
4

Figure 2: Eigenfunctions and computed Wannier functions for a simple one-dimensional model problem. (a) An example eigenfunction plotted on the whole domain, (b) the isolated case, (c) entangled case 1, and (d) entangled case 2. For the three examples of functions computed by the SCDM method we have zoomed in on the region where the bulk of the function is supported.

Bloch-Floquet theory

To facilitate further discussion we briefly review Bloch-Floquet theory for crystal structures. Without loss of generality we consider a three-dimensional crystal. The *Bravis lattice* with lattice vectors $\mathbf{a}_1, \mathbf{a}_2, \mathbf{a}_3 \in \mathbb{R}^3$ is defined as

$$\mathbb{L} = \{\mathbf{R} | \mathbf{R} = n_1\mathbf{a}_1 + n_2\mathbf{a}_2 + n_3\mathbf{a}_3, \quad n_1, n_2, n_3 \in \mathbb{Z}\}. \tag{10}$$

The the potential V is real-valued and $\mathbb{L}$-periodic, *i.e.* $V(\mathbf{r}+n_i\mathbf{a}_i) = V(\mathbf{r}), \quad \forall \mathbf{r} \in \mathbb{R}^3, n_i \in \mathbb{Z}$. The unit cell is defined as

$$\Gamma = \{\mathbf{r} = c_1\mathbf{a}_1 + c_2\mathbf{a}_2 + c_3\mathbf{a}_3 | -1/2 \leq c_1, c_2, c_3 < 1/2\}. \tag{11}$$

The Bravis lattice induces a reciprocal lattice $\mathbb{L}^*$, and the unit cell of the reciprocal lattice is called the (first) *Brillouin zone* and denoted by Γ^*. The problem formulation in the previous section can be formally identified as a special case of this setup with an infinitely large unit cell.

According to the Bloch-Floquet theory, the spectrum of $\mathcal{H}$ can be relabeled using two indices $(b, \mathbf{k})$, where $b \in \mathbb{N}$ is the called the band index and $\mathbf{k} \in \Gamma^*$ is the Brillouin zone index. Each generalized eigenfunction $\psi_{b,\mathbf{k}}(\mathbf{r})$ is known as a Bloch orbital and satisfies $\mathcal{H}\psi_{b,\mathbf{k}}(\mathbf{r}) = \varepsilon_{b,\mathbf{k}}\psi_{b,\mathbf{k}}(\mathbf{r})$. Furthermore, $\psi_{b,\mathbf{k}}$ can be decomposed as $\psi_{b,\mathbf{k}}(\mathbf{r}) = e^{i\mathbf{k}\cdot\mathbf{r}}u_{b,\mathbf{k}}(\mathbf{r})$, where $u_{b,\mathbf{k}}(\mathbf{r})$ is a periodic function with respect to $\mathbb{L}$. An eigenpair $(\varepsilon_{b,\mathbf{k}}, u_{b,\mathbf{k}})$ can be obtained by solving the eigenvalue problem

$$\mathcal{H}(\mathbf{k})u_{b,\mathbf{k}} = \varepsilon_{b,\mathbf{k}}u_{b,\mathbf{k}}(\mathbf{r}), \quad \mathbf{r} \in \Gamma, \quad \mathbf{k} \in \Gamma^*, \tag{12}$$

where $\mathcal{H}(\mathbf{k}) = -\frac{1}{2}(\nabla + i\mathbf{k})^2 + V(\mathbf{r})$. For each $\mathbf{k}$, the eigenvalues $\varepsilon_{b,\mathbf{k}}$ are ordered non-decreasingly. For a fixed b, $\{\varepsilon_{b,\mathbf{k}}\}$ as a function of $\mathbf{k}$ is called a *band*. The collection of all

eigenvalues are called the *band structure* of the crystal, which characterizes the spectrum of the operator $\mathcal{H}$. In this framework, the isolation condition (2) becomes

$$\inf|\varepsilon_{b,\mathbf{k}} - \varepsilon_{b',\mathbf{k}'}| > 0, \quad \mathbf{k},\mathbf{k}' \in \Gamma^*, \varepsilon_{b,\mathbf{k}} \in \mathcal{I}, \varepsilon_{b',\mathbf{k}'} \notin \mathcal{I}. \tag{13}$$

Wannier functions for crystals and disentanglement

Mirroring our prior discussion, we first we consider the isolated case. Without loss of generality we assume the eigenvalues in $\mathcal{I}$ are labeled as $\{\varepsilon_{b,\mathbf{k}}\}_{b=1}^{N_b}$. If we rotate $\{\psi_{b,\mathbf{k}}\}$ by an arbitrary unitary matrix, now indexed by $\mathbf{k}$, $U(\mathbf{k}) \in \mathbb{C}^{N_b \times N_b}$, we can define a new set of functions

$$\widetilde{\psi}_{b,\mathbf{k}}(\mathbf{r}) = \sum_{b'=1}^{N_b} \psi_{b',\mathbf{k}}(\mathbf{r})U_{b',b}(\mathbf{k}), \quad \mathbf{k} \in \Gamma^*. \tag{14}$$

A given set of of matrices $\{U(\mathbf{k})\}$ is called a *gauge*. For any choice of gauge, the Wannier functions for crystals are [30]

$$w_{b,\mathbf{R}}(\mathbf{r}) = \frac{1}{|\Gamma^*|} \int_{\Gamma^*} \widetilde{\psi}_{b,\mathbf{k}}(\mathbf{r})e^{-\imath\mathbf{k}\cdot\mathbf{R}}\,\mathrm{d}\mathbf{k}, \quad \mathbf{r} \in \mathbb{R}^3, \mathbf{R} \in \mathbb{L}, \tag{15}$$

where $|\Gamma^*|$ is the volume of the Brillouin zone. For a class of $\mathcal{H}$ there exists a gauge such that $\widetilde{\psi}_{b,\mathbf{k}}$ is analytic in $\mathbf{k}$, implying that each Wannier function decays exponentially as $|\mathbf{r}| \to \infty$ [2, 27]. Furthermore, the set of Wannier functions $\{w_{b,\mathbf{R}}(\mathbf{r})\}$ forms an orthonormal basis of the subspace in $L^2(\mathbb{R}^3)$ spanned by the Bloch orbitals associated with eigenvalues in $\mathcal{I}$. For crystals, the Wannier localization problem is thus partly reduced to the problem of finding a gauge such that $\widetilde{\psi}_{b,\mathbf{k}}$ is smooth with respect to $\mathbf{k}$. This can be done by minimizing the "spread functional" [22]

$$\Omega[\{w_{b,\mathbf{0}}\}_{b=1}^{N_b}] = \sum_{b=1}^{N} \int |w_{b,\mathbf{0}}(\mathbf{r})^2|\mathbf{r}^2\,\mathrm{d}\mathbf{r} - \left(\int |w_{b,\mathbf{0}}(\mathbf{r})^2|\mathbf{r}\,\mathrm{d}\mathbf{r}\right)^2. \tag{16}$$

Only $\mathbf{R} = \mathbf{0}$ is considered because Wannier functions associated with different $\mathbf{R}$'s only differ by translation.

In the entangled case, the disentanglement method constructs the gauge via a two-step procedure. It first finds a gauge $U^{\mathrm{dis}}(\mathbf{k}) \in \mathbb{C}^{N_b \times N_w}$, in order to disentangle the given set of N_b functions into N_w functions for each $\mathbf{k}$. This is obtained by maximizing a "smoothness functional" [29] with respect to $\mathbf{k}$ for the following auxiliary functions

$$\psi_{b,\mathbf{k}}^{\mathrm{dis}}(\mathbf{r}) = \sum_{b'=1}^{N_b} \psi_{b',\mathbf{k}}(\mathbf{r})U_{b',b}^{\mathrm{dis}}(\mathbf{k}), \quad b = 1,\ldots,N_w, \mathbf{k} \in \Gamma^*. \tag{17}$$

After obtaining $U^{\mathrm{dis}}(\mathbf{k})$ a second gauge $U^{\mathrm{loc}}(\mathbf{k}) \in \mathbb{C}^{N_w \times N_w}$ for each $\mathbf{k}$ is computed by minimizing the spread functional (16). Finally, the overall gauge in the disentanglement method is the composition $U(\mathbf{k}) = U^{\mathrm{dis}}(\mathbf{k})U^{\mathrm{loc}}(\mathbf{k})$.

This two-step procedure can be viewed as a heuristic means to solve a nonlinear, nonconvex multi-objective optimization problem aiming to simultaneously maximize the smoothness functional with respect to $\mathbf{k}$, and minimize the spread functional. Our numerical results indicate that, at least in some cases, this two step procedure may not be an effective surrogate for the desired optimization problem.

SCDM for crystals

We now proceed to discuss the relatively minor modifications needed to generalize the SCDM method to crystals.

In the isolated case, for each $\mathbf{k}$-point in the Brillouin zone the $\mathbf{k}$-dependent density matrix is gauge invariant

$$P(\mathbf{k}) = \sum_{\varepsilon_{b,\mathbf{k}} \in \mathcal{I}} |\psi_{b,\mathbf{k}}\rangle\langle\psi_{b,\mathbf{k}}| = \sum_{\varepsilon_{b,\mathbf{k}} \in \mathcal{I}} |\widetilde{\psi}_{b,\mathbf{k}}\rangle\langle\widetilde{\psi}_{b,\mathbf{k}}|, \tag{18}$$

and is already an analytic function of $\mathbf{k}$ [25, 27]. The SCDM method uses the density matrix to construct a gauge so that $\widetilde{\psi}_{b,\mathbf{k}}$ is smooth with respect to $\mathbf{k}$. However, for crystals, we need to select a common set of columns for all the $\mathbf{k}$-dependent density matrices. Previous work [7] suggests that it is often sufficient to select the columns using an "anchor" point $\mathbf{k}_0$, such as the so-called Gamma-point $(0,0,0)^T$ to identify these columns. A generalization of this procedure is also outlined in [7], though in our numerical experiments we have found use of the Gamma-point as the anchor point suffices.

Let $\Psi_{\mathbf{k}} \in \mathbb{C}^{N_g \times N_b}$ be the unitary matrix representing $\{\psi_{b,\mathbf{k}}(\mathbf{r})\}$ on a discrete grid in the unit cell. At the anchor point $\mathbf{k}_0$, we compute the QRCP $\Psi_{\mathbf{k}_0}^* \Pi = QR$. As before, let $\mathcal{C} = \{\mathbf{r}_b\}_{b=1}^{N_b}$ denote the grid points corresponding to the N_b selected columns where $\mathbf{r}_b \in \Gamma$. For each $\mathbf{k}$ point, define the auxiliary matrix $\Xi \in \mathbb{C}^{N_b \times N_b}$ with matrix elements $\Xi_{b,b'}(\mathbf{k}) = \psi_{b,\mathbf{k}}^*(\mathbf{r}_{b'})$. Then the smoothness of the density matrix $P(\mathbf{k})$ implies that each function $P_{b,\mathbf{k}}(\mathbf{r}) = \sum_{b'=1}^{N_b} \psi_{b',\mathbf{k}}(\mathbf{r})\Xi_{b',b}(\mathbf{k})$ is smooth with respect to $\mathbf{k}$. As before the SCDM gauge can be constructed via the Löwdin transformation as

$$U(\mathbf{k}) = \Xi(\mathbf{k}) \left[\Xi^*(\mathbf{k})\Xi(\mathbf{k})\right]^{-\frac{1}{2}}. \tag{19}$$

Similar to Eq. (5),

$$(\Xi^*(\mathbf{k})\Xi(\mathbf{k}))_{b,b'} = \sum_{b''=1}^{N_b} \psi_{b'',\mathbf{k}}(\mathbf{r}_b)\psi_{b'',\mathbf{k}}^*(\mathbf{r}_{b'}) = P(\mathbf{r}_b, \mathbf{r}_{b'}; \mathbf{k}). \tag{20}$$

Since the kernel $P(\mathbf{r}_b, \mathbf{r}_{b'}; \mathbf{k})$ is smooth with respect to $\mathbf{k}$, the matrix $(\Xi^*(\mathbf{k})\Xi(\mathbf{k}))^{-\frac{1}{2}}$ is smooth with respect to $\mathbf{k}$ as long as the eigenvalues of $[\Xi^*(\mathbf{k})\Xi(\mathbf{k})]$ are uniformly bounded away from 0 for $\mathbf{k}$ in the Brillouin zone. As a result,

$$\widetilde{\psi}_{b,\mathbf{k}}(\mathbf{r}) = \sum_{b'=1}^{N_b} \psi_{b',\mathbf{k}}(\mathbf{r})U_{b',b}(\mathbf{k}) = \sum_{b'=1}^{N_b} P_{b',\mathbf{k}}(\mathbf{r}) \left[\Xi^*(\mathbf{k})\Xi(\mathbf{k})\right]_{b',b}^{-\frac{1}{2}} \tag{21}$$

is smooth with respect to $\mathbf{k}$. Therefore, the Fourier transform of $\widetilde{\psi}_{b,\mathbf{k}}$ with respect to $\mathbf{k}$ as in Eq. (15) gives rise to the Wannier functions for crystals constructed by the SCDM method.

In the entangled case (when (13) is not satisfied), the SCDM method makes use of a $\mathbf{k}$-dependent quasi-density matrix for each $\mathbf{k}$ point:

$$P(\mathbf{k}) = \sum_{\varepsilon_{b,\mathbf{k}}} |\psi_{b,\mathbf{k}}\rangle f(\varepsilon_{b,\mathbf{k}})\langle\psi_{b,\mathbf{k}}|. \tag{22}$$

Here, the choice of $f(\varepsilon)$ matches what we previously discussed, and depends on the desired $\mathcal{I}$. In particular, the reduction to the isolated case is again the choice $f(\varepsilon) = \mathbf{1}_{\mathcal{I}}(\varepsilon)$, which reduces the $\mathbf{k}$-dependent quasi-density matrix to a $\mathbf{k}$-dependent density matrix. Numerical results indicate that these quasi-density matrices for the two entangled cases are smooth with respect to $\mathbf{k}$.

Let $\mathcal{E}(\mathbf{k}) = \text{diag}\left[\{\varepsilon_{b,\mathbf{k}}\}_{b=1}^{N_b}\right]$ be a diagonal matrix for each $\mathbf{k}$ containing eigenvalues such that $f(\varepsilon)$ is larger than some threshold. Computing a QRCP at the anchor point in the Brillouin zone $\mathbf{k}_0$, we obtain

$$f(\mathcal{E}(\mathbf{k}_0))\Psi_{\mathbf{k}_0}^*\Pi = QR. \tag{23}$$

Analogously to before, the set of real space points $\mathcal{C} = \{\mathbf{r}_b\}_{b=1}^{N_w}$ are given by the left most N_w columns of the permutation matrix Π. If we define the auxiliary matrix $\Xi(\mathbf{k}) \in \mathbb{C}^{N_b \times N_w}$ with matrix elements $\Xi_{b,b'}(\mathbf{k}) = f(\varepsilon_{b,\mathbf{k}})\psi_{b,\mathbf{k}}^*(\mathbf{r}_{b'})$, $P_{b,\mathbf{k}}(\mathbf{r}) = \sum_{b'} \psi_{b',\mathbf{k}}(\mathbf{r})\Xi_{b',b}(\mathbf{k})$ is smooth with respect to $\mathbf{k}$. If the eigenvalues of $[\Xi^*(\mathbf{k})\Xi(\mathbf{k})]$ are uniformly bounded away from 0 in the Brillouin zone, the gauge $U(\mathbf{k}) \in \mathbb{C}^{N_b \times N_w}$ given by Eq. (19) is unitary and via (21) defines $\{\widetilde{\psi}_{b,\mathbf{k}}\}$ that are smooth with respect to $\mathbf{k}$. Eq. (15) once again yields the desired Wannier functions.

Numerical results

We now demonstrate the effectiveness of the SCDM method qualitatively and quantitatively using real materials. The electronic structure calculations are performed using the QUANTUM ESPRESSO [9] software package with the PBE exchange-correlation functionals [28].

Qualitatively, we examine the shape of the Wannier functions obtained from SCDM, and compare against minimizer of the spread functional (16) in `Wannier90`. Quantitatively, we measure the value of the spread functional for Wannier functions obtained from SCDM, as well as the accuracy of band structure interpolation from the Wannier functions for isolated and entangled cases. Practically, the Brillouin zone needs to be discretized using a finite number of points. However, $\varepsilon_{b,\mathbf{k}}$ as a function of $\mathbf{k}$ often needs to be computed on finely discretized paths through the Brillouin zone that do not coincide with the discretization grid—this is band structure (or Wannier) interpolation. We built an interface for our method to the widely used `Wannier90` software package [23] allowing us to use its interpolation routines. Details of this procedure and our interface with `Wannier90` may be found in the supporting information and our code is available online[1].

Our first example is a Cr_2O_3 crystal with collinear spin polarization. Each unit cell has 92 occupied bands and we are interested in the top 6 valence bands, corresponding to 3 spin-up and 3 spin-down d orbitals for the Cr atoms. This is a challenging system for `Wannier90` due to the existence of multiple local minima in the spread functional and the convergence of existing methods can depend sensitively on the choice of the initial guess. For example, in Fig. 3a, when the initial guess is given by projections corresponding to d_{xy}, d_{yz} and d_{xz} orbitals respectively, the spread functional decreases from 70.56Å^2 to 16.99Å^2 within 30 steps. In contrast, when the initial guess is given by sp^2 hybridized orbitals the spread functional starts at 193.94Å^2 and stops decreasing around 47.13Å^2, indicating that the optimization procedure is trapped at a stationary point. On the other hand, starting

---

[1]`https://github.com/asdamle/SCDM`

from the SCDM initial guess, the spread starts at 17.22Å^2 and quickly converges to 16.98Å^2. Fig. 3b plots the atomic configuration and isosurface of a localized spin-up orbital obtained from the SCDM gauge without further Wannier optimization. The SCDM localized orbitals clearly demonstrate d orbital character without relying on a user specified initial guess.
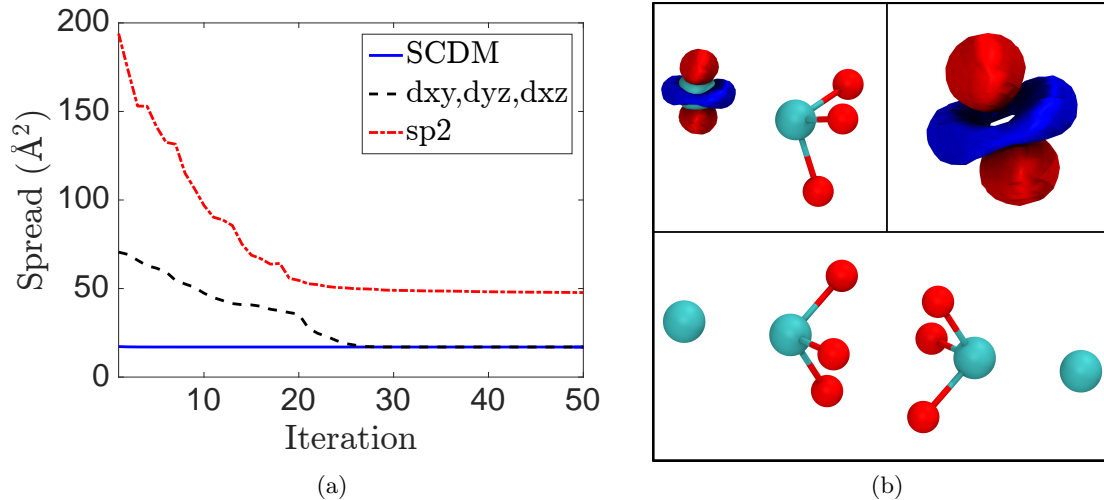

(a)   (b)

Figure 3: (color online) (a) Convergence of the spread for Cr_2O_3 starting from the initial guess of the gauge matrix from SCDM (blue solid line), initial guess from d orbitals (black dashed line) and initial guess from sp^2 orbitals (red dotted line). (b) One unit cell of Cr_2O_3, and the shape of a localized function obtained from SCDM (plot generated using Visual Molecular Dynamics [14]). The localized function has been plotted with and without the molecular structure to better illustrate its character and physical location.

Next, we consider two examples with entangled eigenvalues. Fig. 4a shows band structure interpolation for a Si crystal with 8 localized functions computed from SCDM. This corresponds to entangled case 1 ,covering both valence bands and low-lying conduction bands. We set $\mu = 10.0$ eV, $\sigma = 2.0$ eV, and use a $10 \times 10 \times 10$ **k**-point grid for constructing the Wannier functions. Fig. 4b shows the accuracy of band structure interpolation for a Cu crystal with 7 localized functions. This corresponds to the entangled case 2, covering valence bands near the Fermi energy contributed mainly from the d-orbitals. We use $\mu = 15.5$ eV, $\sigma = 4.0$ eV, and a $10 \times 10 \times 10$ **k**-point grid. In both cases, the SCDM method accurately reproduces the band structure within the energy window of interest.

We now turn to graphene, a metallic system that is particularly challenging for band structure interpolation due to the linear band structure near the Dirac point. Fig. 5 demonstrates that SCDM can accurately interpolate the band structure of graphene even when zooming in on the region near the Dirac point. We set $\mu = -2.5$ eV $\sigma = 4.0$ eV, and use a $12 \times 12 \times 1$ **k**-grid for constructing the Wannier functions.

Finally, we measure the convergence rate of the band structure interpolation with respect to an increasing number of **k**-points using Wannier functions obtained from SCDM and those from a (local) minimum corresponding to the optimization objective in `Wannier90`. Fig. 6a reports the absolute value of the error of the eigenvalues for the occupied bands of Si. The chosen path through the Brillouin zone is discretized with 408 points. A cubic $k \times k \times k$ grid is used and k ranges from 4 to 14. Both the average and the maximum value
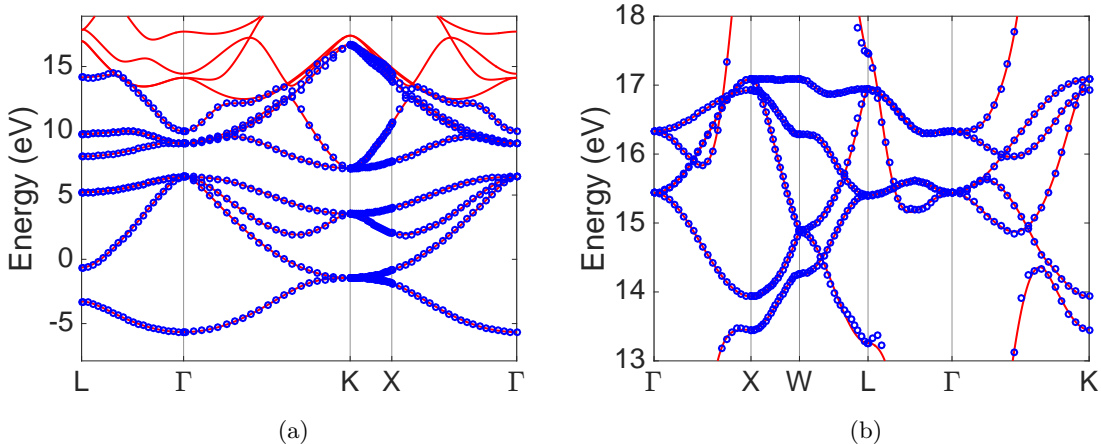
Figure 4: (color online) Wannier interpolation with SCDM for the band structure for (a) valance and conduction bands for Si (b) bands near the Fermi energy for Cu. Direct calculation (red line) and SCDM based Wannier interpolation (blue circles).

of the error converge exponentially with respect to k. For the isolated case, the error with the optimized gauge matrix is slightly smaller than that with the SCDM gauge matrix. However, we find that visually the Wannier functions from SCDM with a $6 \times 6 \times 6$ **k**-grid already result in excellent band structure.

Fig. 6b reports the absolute value of the error of the eigenvalues below the Fermi energy for Al, which is a metallic system with entangled band structure. The chosen path in the Brillouin zone is discretized into 510 points. A cubic $k \times k \times k$ grid is used and k ranges from 6 to 16. We use the erfc smearing with μ being the chemical potential at 8.4 eV, and $\sigma = 4.0$ eV. We compute six bands for each **k** point and SCDM picks the leading four bands. Even for metallic system, numerical results show exponential convergence of the band structure interpolation. Fig. 7a shows that Wannier interpolation using the SCDM gauge matrix with a $10 \times 10 \times 10$ **k**-grid already yields excellent band structure. In particular, using the SCDM gauge correctly reproduces band crossings even though a relatively coarse **k** grid is used.

For this metallic system, the error of the eigenvalues interpolated using the SCDM gauge matrix is systematically smaller than that of the optimized gauge matrix from `Wannier90`. Therefore optimization of the spread functional alone does not necessarily improve the interpolation quality. This assessment is further justified by performing Wannier interpolation with a gauge matrix obtained by minimizing the Wannier spread functional directly using six bands and using four orbitals that have sp^3 character for the initial guess. In this case the optimized spread is 12.42Å^2, while the SCDM gauge gives a larger spread of 18.38Å^2. However, Fig. 7b shows that the band structure obtained using the optimized gauge with the sp^3 initial guess is significantly less accurate when compared to that in Fig. 7a even though the same **k** grid is used. In particular, the spread functional alone is not necessarily a proxy for interpolation quality. On the other hand, the SCDM method obtains a smooth density matrix for the range of the required band energies by construction.
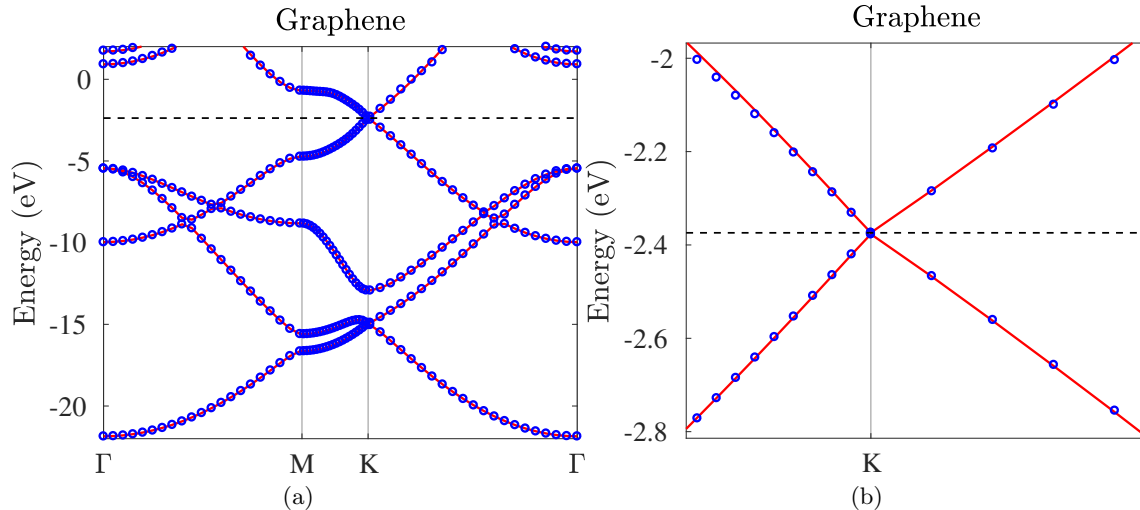
Figure 5: (color online) Wannier interpolation with SCDM for the band structure for graphene (a) below the Fermi energy (b) near the Dirac point. Direct calculation (red lines) and SCDM based Wannier interpolation (blue circles).

Discussion and conclusion

We developed a unified method to compute Wannier functions for systems with both isolated and entangled bands. Its simplicity—in both implementation and reliance on few parameters—makes it easy to use. Of particular importance, our method removes the potentially sensitive dependence of the construction of Wannier functions on an initial guess to a nonconvex optimization (two-stage in the entangled case) procedure. This potentially makes it easier to treat complicated materials where the choice of a good guess may be difficult, and convergence to local minima may hamper the construction of localized Wannier functions. Interestingly, even though we do not seed our method with a physically informed initial guess, we are able to recover physically interpretable Wannier functions. Furthermore, as we have shown, the objective function of the existing optimization procedure is not necessarily a proxy for good band interpolation. Collectively, these qualities and observations make our new SCDM methodology attractive for the construction of Wannier functions.
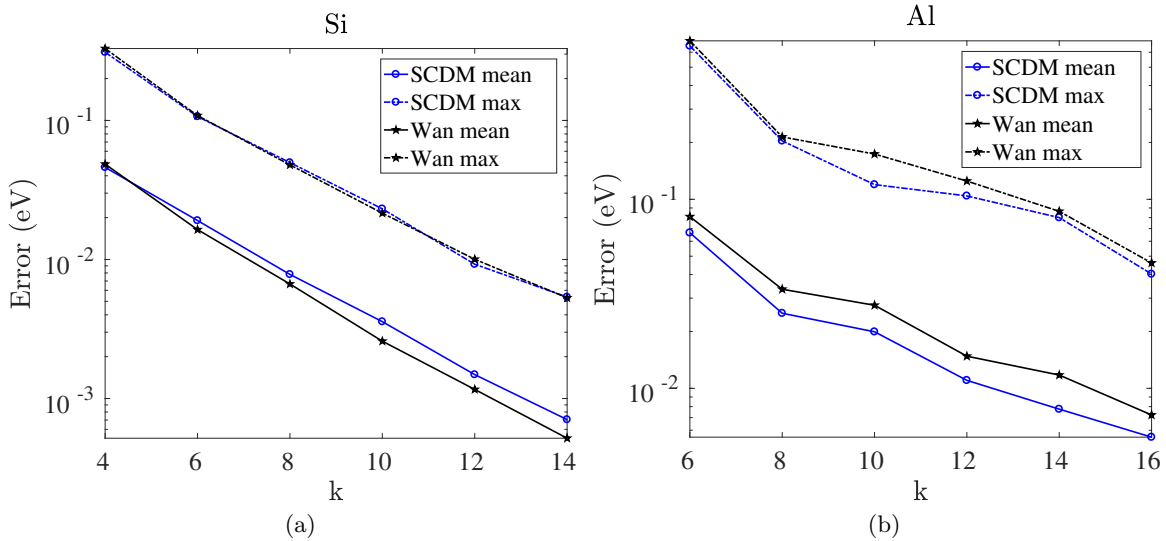
Acknowledgments

Figure 6: (color online) Convergence of the average and maximum error of Wannier interpolation below the Fermi energy using the SCDM gauge matrix, and converged Wannier gauge matrix starting from the SCDM initial guess for (a) silicon (b) aluminum.

References

[1] M. Benzi, P. Boito, and N. Razouk. Decay properties of spectral projectors with applications to electronic structure. *SIAM Rev.*, 55:3–64, 2013.

[2] E. I. Blount. Formalisms of band theory. *Solid State Ohys.*, 13:305–373, 1962.

[3] D. R. Bowler and T. Miyazaki. O(N) methods in electronic structure calculations. *Rep. Prog. Phys.*, 75:036503, 2012.

[4] C. Brouder, G. Panati, M. Calandra, C. Mourougane, and N. Marzari. Exponential localization of Wannier functions in insulators. *Phys. Rev. Lett.*, 98:046402, 2007.

[5] E. Cancès, A. Levitt, G. Panati, and G. Stoltz. Robust determination of maximally-localized Wannier functions. *Phys. Rev. B*, 95:075114, 2017.

[6] A. Damle, L. Lin, and L. Ying. Compressed representation of Kohn–Sham orbitals via selected columns of the density matrix. *J. Chem. Theory Comput.*, 11(4):1463–1469, 2015.

[7] Anil Damle, Lin Lin, and Lexing Ying. Scdm-k: Localized orbitals for solids via selected columns of the density matrix. *J. Comput. Phys.*, 334:1 – 15, 2017.

[8] W. E, T. Li, and J. Lu. Localized bases of eigensubspaces and operator compression. *Proc. Natl. Acad. Sci.*, 107(4):1273–1278, 2010.

[9] Paolo Giannozzi, Stefano Baroni, Nicola Bonini, Matteo Calandra, Roberto Car, Carlo Cavazzoni, Davide Ceresoli, Guido L Chiarotti, Matteo Cococcioni, Ismaila Dabo, Andrea Dal Corso, Stefano de Gironcoli, Stefano Fabris, Guido Fratesi, Ralph Gebauer,
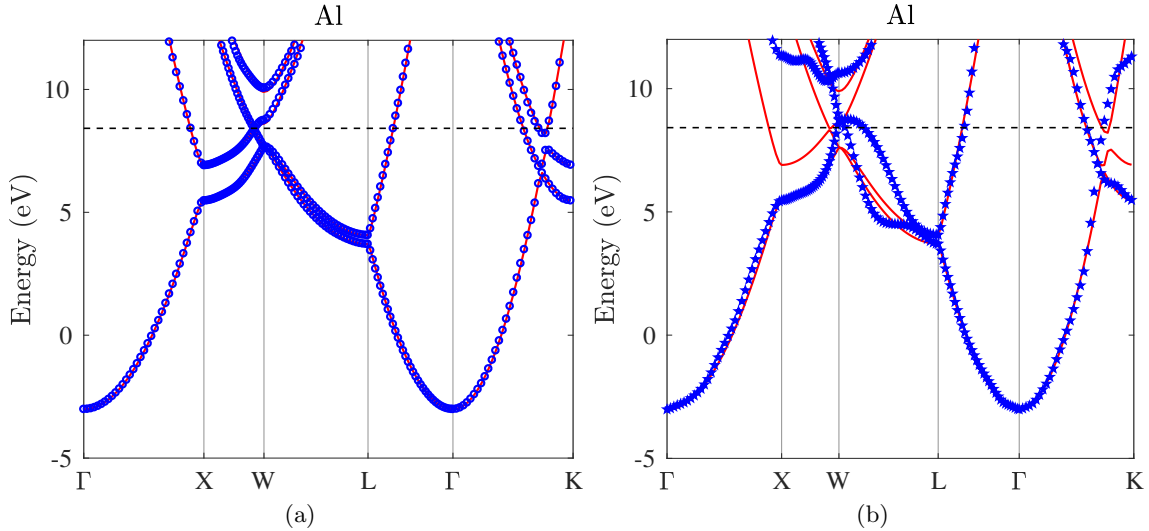
Figure 7: (color online) (a) Band structure for Al around and below the Fermi energy (black dashed line). Direct calculation from QE (red line), and Wannier interpolation using SCDM gauge matrix with a $10 \times 10 \times 10$ **k**-grid (blue circle). (b) Same calculation but using the Wannier gauge matrix starting from an sp^3 initial guess with $N_b = 6, N_w = 4$.

Uwe Gerstmann, Christos Gougoussis, Anton Kokalj, Michele Lazzeri, Layla Martin-Samos, Nicola Marzari, Francesco Mauri, Riccardo Mazzarello, Stefano Paolini, Alfredo Pasquarello, Lorenzo Paulatto, Carlo Sbraccia, Sandro Scandolo, Gabriele Sclauzero, Ari P Seitsonen, Alexander Smogunov, Paolo Umari, and Renata M Wentzcovitch. QUANTUM ESPRESSO: a modular and open-source software project for quantum simulations of materials. *J. Phys.: Condens. Matter*, 21:395502–395520, 2009.

[10] S. Goedecker. Linear scaling electronic structure methods. *Rev. Mod. Phys.*, 71:1085–1123, 1999.

[11] G. H. Golub and C. F. Van Loan. *Matrix computations*. Johns Hopkins Univ. Press, Baltimore, fourth edition, 2013.

[12] F. Gygi. Compact representations of Kohn–Sham invariant subspaces. *Phys. Rev. Lett.*, 102:166406, 2009.

[13] P. Hohenberg and W. Kohn. Inhomogeneous electron gas. *Phys. Rev.*, 136:B864–B871, 1964.

[14] William Humphrey, Andrew Dalke, and Klaus Schulten. VMD – Visual Molecular Dynamics. *Journal of Molecular Graphics*, 14:33–38, 1996.

[15] E. Koch and S. Goedecker. Locality properties and Wannier functions for interacting systems. *Solid State Commun.*, 119:105, 2001.

[16] W. Kohn. Analytic properties of Bloch waves and Wannier functions. *Phys. Rev.*, 115:809, 1959.

[17] W. Kohn. Density functional and density matrix method scaling linearly with the number of atoms. *Phys. Rev. Lett.*, 76:3168–3171, 1996.

[18] W. Kohn and L. Sham. Self-consistent equations including exchange and correlation effects. *Phys. Rev.*, 140:A1133–A1138, 1965.

[19] L. Lin. Localized spectrum slicing. *Math. Comp.*, in press.

[20] P.-O. Löwdin. On the non-orthogonality problem connected with the use of atomic wave functions in the theory of molecules and crystals. *J. Chem. Phys.*, 18:365–375, 1950.

[21] N. Marzari, A. A. Mostofi, J. R. Yates, I. Souza, and D. Vanderbilt. Maximally localized Wannier functions: Theory and applications. *Rev. Mod. Phys.*, 84:1419–1475, 2012.

[22] N. Marzari and D. Vanderbilt. Maximally localized generalized Wannier functions for composite energy bands. *Phys. Rev. B*, 56(20):12847, 1997.

[23] A.A. Mostofi, J.R. Yates, Y.S. Lee, I. Souza, D. Vanderbilt, and N. Marzari. Wannier90: a tool for obtaining maximally-localised wannier functions. *Comput. Phys. Commun.*, 178:685, 2008.

[24] J. I. Mustafa, S. Coh, M. L. Cohen, and S. G. Louie. Automated construction of maximally localized Wannier functions: Optimized projection functions method. *Phys. Rev. B*, 92:165134, 2015.

[25] G. Nenciu. Dynamics of band electrons in electric and magnetic fields: rigorous justification of the effective hamiltonians. *Rev. Mod. Phys.*, 63:91–127, Jan 1991.

[26] V. Ozoliņš, R. Lai, R. Caflisch, and S. Osher. Compressed modes for variational problems in mathematics and physics. *Proc. Natl. Acad. Sci.*, 110(46):18368–18373, 2013.

[27] G. Panati and A. Pisante. Bloch bundles, Marzari-Vanderbilt functional and maximally localized Wannier functions. *Commun. Math. Phys.*, 322:835–875, 2013.

[28] J. P. Perdew, M. Ernzerhof, and K. Burke. Rationale for mixing exact exchange with density functional approximations. *J. Chem. Phys.*, 105:9982–9985, 1996.

[29] I. Souza, N. Marzari, and D. Vanderbilt. Maximally localized wannier functions for entangled energy bands. *Phys. Rev. B*, 65:035109, 2001.

[30] G. H. Wannier. The structure of electronic excitation levels in insulating crystals. *Phys. Rev.*, 52:191, 1937.

[31] J. R. Yates, X. Wang, D. Vanderbilt, and I. Souza. Spectral and Fermi surface properties from Wannier interpolation. *Phys. Rev. B*, 75:195121, 2007.